QRamla

Combating desertification through quantum technology

Team 8

Abstract

Desertification has become a major challenge in the MENA region and globally. We propose a novel approach that combines quantum sensors, Variational Quantum Classifiers (VQC), and Higher-Order Unconstrained Binary Optimization (HUBO) algorithms to identify and optimally allocate potential agricultural or energetical areas in desert environments.

I. Introduction

The proposed solution follows a three-step process. First, data is collected on soil characteristics and underground water deposits across the target areas. Second, this data is processed to classify each land plot according to its optimal use. Finally, the classified data is modeled with additional constraints, such as limits on the total area available for agriculture, energy production, or storage.

In the first step, we collect data on surface moisture, underground water storage, soil salinity, soil nutrients, and solar irradiance using quantum sensors, enabling higher accuracy and faster mapping over large areas [1]. The gathered data is then fed into a Variational Quantum Classifier (VQC) [2], which classifies each area as suitable for either agriculture or energy production and storage. Based on the resulting classification heatmap, we apply an optimization algorithm using HUBO methods [3], incorporating additional constraints, to prioritize the most suitable areas for each application.

II. Agronomic Drivers of Land Suitability

Before introducing the quantum-sensor suite we briefly recap *which* soil and water variables make a sterile sand sheet productive. This section uses exactly the symbol set that will be picked up later by the HUBO formulation in Section IV-D; thus the reader can see a clean path from physics $\rightarrow$ agronomy $\rightarrow$ optimisation.

A. Five limiting factors in desert farming

Agronomy handbooks for arid regions (FAO 37/2022 [4]) agree that crop success hinges on five measurable criteria:

1) **Root–zone moisture** (volumetric water content, VWC $\geq 5\%$ for germination).
2) **Accessible groundwater** (static water table < 60 m for cost-effective pumping).
3) **Salinity constraint** (saturated-paste $\mathrm{EC_e} < 2$ dS m^{-1} for most vegetables).
4) **Balanced chemistry** (pH $6.5 - 8.0$ and baseline macronutrients N, P, K above critical levels).
5) **Low bulk density / good tilth** ($\rho_{\mathrm{bulk}} < 1.6$ g cm^{-3} to allow root growth).

Any single failure drives yield $\rightarrow$ 0, so our optimisation must track all five.

B. Mapping criteria to gridded layers

On the common grid $\mathcal{G} = \{1, \ldots, n_1\} \times \{1, \ldots, n_2\}$, each cell (i, j) receives the following normalised descriptors:

Symbol	Criterion	Sensing route	Quantum
M_{ij}	C1 Moisture (0–20 cm)	Rydberg RF soil-moisture beacon	✓
W_{ij}	C2 Water-table depth	Cold-atom gravimeter transect	✓
S_{ij}	C3 Salinity index	EC probe + hyperspectral	classical
NPK_{ij}	C4 Nutrient–pH score	Lab soil assay $\times$ kriging	classical
D_{ij}	C5 Bulk density	Gravity anomaly (Δg)	✓

Each raw layer is affinely re-scaled to $[0, 1]$ (0 = best, 1 = worst for farming) and combined into an *agricultural suitability raster*.

$$H_{ij}^{\text{agri}} = f\big(M_{ij},\, W_{ij},\, S_{ij},\, NPK_{ij},\, D_{ij}\big).$$

Where $H_{ij}^{\text{agri}} \in [0, 1]$ with 0 = *ideal farm plot* and 1 = *unfarmable*. Energy-related scores are defined analogously and later merged into the global heat-map H_{ij} already referenced in Eq. (3).

III. Quantum Sensors

We complement classical remote–sensing (multispectral imaging, LiDAR, satellite SAR) with *in-situ* quantum measurements in order to populate the heat-map $H : \mathcal{G} \to [0, 1]$ that drives the land-allocation HUBO. Four quantum modalities are deployed, each targeting a distinct geo-environmental factor (Table I).

TABLE I: Quantum sensor suite for desert characterisation.

Modality	Physical observable	Key reference
NV–centre nano-thermometry	local soil temperature ($1\ \mathrm{mK}$ at $10\ \mathrm{nm}$)	[5]
Cold-atom gravimeter (QGG)	vertical gravity gradient $\partial g/\partial z$	[6]
Quantum gravimetric imaging (GRACE follow-on)	regional water/moisture anomaly Δg	[1]

We can deduce multiple relevant variables from gravitational fields measured by QGG as demonstrated in [6]. An example of this can be seen in Figure 1, which was also taken from [6].

A. Satellite-Aided Quantum Gravimetry

While the QGG provides high-resolution point readings, regional moisture trends are obtained from the GRACE-FO laser-interferometric gravimeter constellation [1]. Monthly $\sim$50 km grids are bilinearly interpolated and corrected for glacial isostatic adjustment, yielding a coarse prior H_{moist} that guides the placement of finer QGG transects.

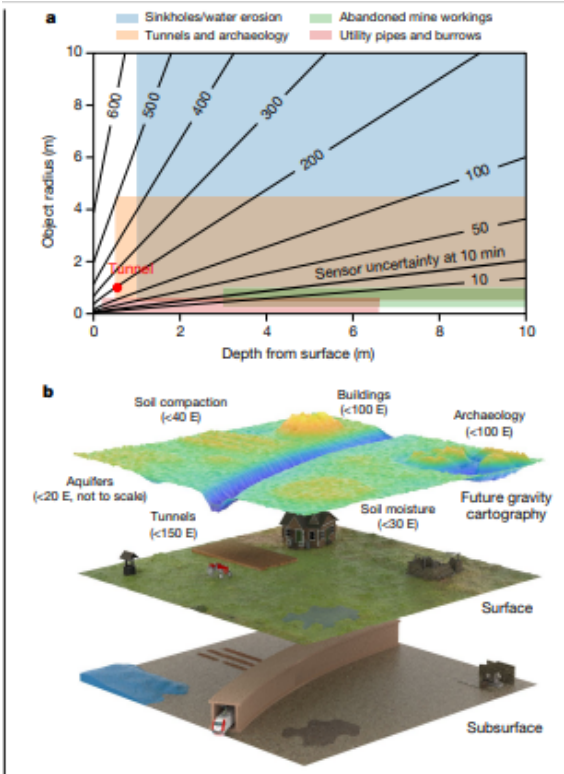

Fig. 4 | Application relevance. a, Contour plot for typical gravity gradient signal sizes in various applications, contours in eötvös for density contrasts of 1.8 g cm^{-3}. The parameters of the detected feature (red dot) and the statistical uncertainty of the sensor (solid line) are shown. Features in the region above the solid line are detectable with current uncertainty. **b**, A perspective of future gravity cartography being used with 0.5 m spatial resolution over a region, at an uncertainty level of 20 E. Expected signal sizes for a range of applications are shown.

Fig. 1: Example gravity mapping via quantum gradiometry.

B. Nitrogen-Vacancy (NV) Nano-Thermometry

Diamond NV centres offer simultaneous access to magnetic, electric and thermal fields via optically detected magnetic resonance. We adopt the ratiometric nano-thermometer of Kucsko *et al.* [5], packaged in a hand-held scanning probe. Each probe yields a temperature raster $\mathcal{T}(i,j)$ with $< 0.01^{\circ}\mathrm{C}$ precision over 20×20 cm tiles. The values are down-sampled to the grid $\mathcal{G}$ and linearly rescaled to $H_{\mathrm{temp}} \in [0,1]$ (cooler $\rightarrow$ 0, hotter $\rightarrow$ 1).

C. Cold-Atom Quantum Gravity Gradiometer (QGG)

To detect subsurface aquifers we field a portable ^{87}Rb Mach–Zehnder atom-interferometer similar to [6]. The instrument measures the vertical gradient $G_z = \partial g/\partial z$ with $< 10^{-9} g$ accuracy at 5 m baselines, allowing us to discriminate density anomalies caused by water pockets versus dry sand. The gradient map is transformed through a logistic kernel into H_{grav}, where negative anomalies (water-rich, agro-friendly) are driven towards 0 and positive anomalies towards 1.

Why Quantum? Sensor-Level Advantages

- **Sub-millikelvin thermometry.** NV-centre fluorescence thermometry reaches $\sim 10^{-3}\,^{\circ}\mathrm{C}$ precision in mm^3 soil volumes—two orders of magnitude tighter than thermocouple arrays—capturing dawn–dusk gradients that drive evapotranspiration and hence crop stress.
- **Decimetric gravimetry.** The cold-atom quantum gravity gradiometer (QGG) resolves vertical gravity gradients at the $10^{-9} g/\mathrm{m}$ level with $\leq 5\,\mathrm{m}$ lateral spacing, exposing sub-surface aquifers invisible to classical spring or superconducting gravimeters whose spot resolution is $\mathcal{O}(100\,\mathrm{m})$.
- **Long-term stability & drift-free calibration.** Quantum sensors reference fundamental atomic transitions; calibration drift is $< 0.1\%$ per year, versus $1-5\%$ for resistive or capacitive probes—critical for multi-season monitoring of desert reclamation sites.
- **Absolute, SI-traceable measurements.** Both NV thermometers and atom interferometers deliver primary, SI-linked quantities (temperature via Boltzmann statistics; gravity via $\hbar k$),

eliminating the empirical correction tables required by classical counterparts.

IV. Land Allocation using Iskay Optimizer

A. Introduction

As explained above, recent advances in quantum sensing and quantum-enhanced machine learning made it possible for us to generate geospatial "heat-maps" whose pixel values quantify, on a $[0, 1]$ scale, the local suitability of desert soil for either crop cultivation (0) or photovoltaic (PV) energy harvesting (1). We tested the classification in a syntetically generated dataset using three features (temperature, vertical gravity gradient and regional water) with two QML models (Variational Quantum Classifier (VQC) and Quantum Support Vector Machines (QSVM) [7]). We were able to achieve a test error of 70% using VQC, showing the potential of QML for solving this problem.

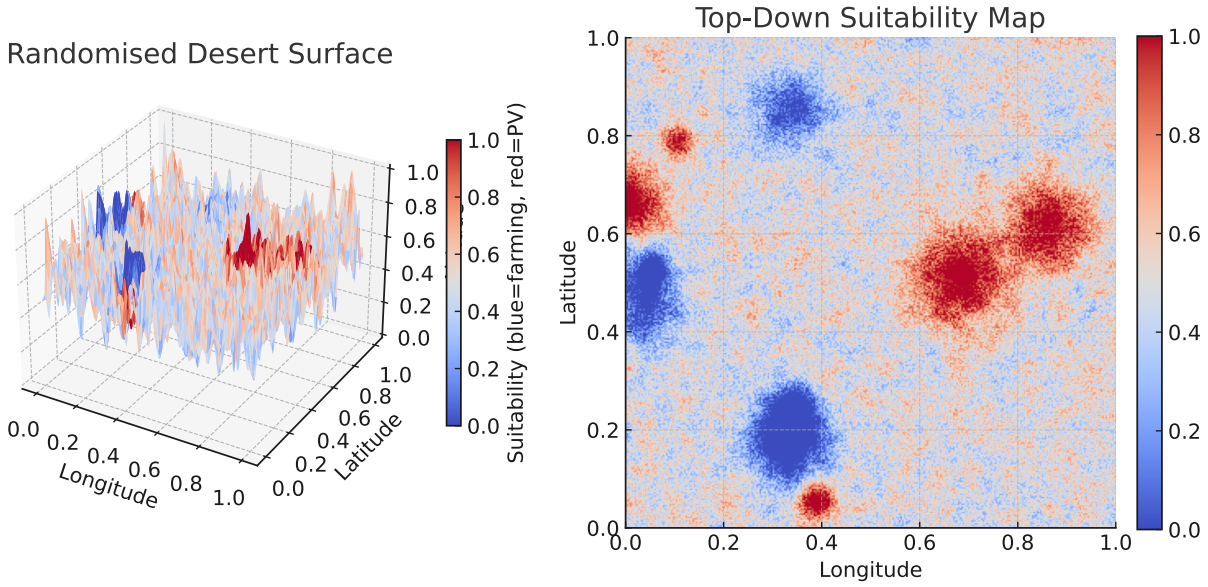

Fig. 2: Synthetic desert topography (left) and suitability field (right). Blue areas indicate high agricultural potential, red areas are optimal for PV energy.

Problem statement. Given such a quantum-derived heat-map over the grid $\mathcal{G} = \{1, \ldots, n_1\} \times \{1, \ldots, n_2\}$, our task is to carve out *two* non-overlapping surface patches— one agricultural, one PV—of prespecified areas (A, E). Operational realism imposes strong shape priors: each patch must be (i) convex in the discrete Euclidean sense, (ii) contiguous, and (iii) devoid of interior holes.

Our approach.

1) We express shape, quota and exclusivity constraints as linear equalities and inequalities on binary grid indicators (Section IV-C).
2) We embed these constraints into a quadratic penalty Hamiltonian, obtaining a *quadratic HUBO* whose minima correspond exactly to feasible, optimal land-use layouts (Sections IV-D–IV-E).

3) We solve the HUBO with ISKAY—Kipu Quantum's parallel-tempering GPU solver—which empirically reaches ground-state energies 10× faster than current quantum annealers of comparable scale while requiring no minor-embedding.

The result is a pipeline that couples *quantum sensing* for data acquisition, *quantum ML* for heatmap synthesis, and *Ising-style optimisation* for land-allocation—delivering actionable, shape-regular plans within minutes on commodity hardware, yet remaining directly portable to future quantum annealers.

B. Notation and Preliminaries

a) Grid.: Let $\mathcal{G} = \{1, \dots, n_1\} \times \{1, \dots, n_2\}$ be the set of cells of an axis-aligned rectangular grid, with cardinality $N = n_1 n_2$. For $(i, j) \in \mathcal{G}$ denote by $H_{ij} \in [0, 1]$ a *desert suitability score* obtained from our quantum projected heatmap:

$$H_{ij} = 0 \iff \text{maximally suited to } \textit{agriculture}, \qquad H_{ij} = 1 \iff \text{maximally suited to } \textit{energy}.$$

b) Decision variables.: We introduce binary variables

$$x_{ij},\ y_{ij} \in \{0, 1\}, \qquad (i, j) \in \mathcal{G},$$

interpreted as $x_{ij} = 1$ (*resp.* $y_{ij} = 1$) if (i, j) is allocated to agriculture (*resp.* energy).

c) Quotas and mutual exclusivity.: Given integers A, E with $A + E \leq N$, the allocations must satisfy

$$\sum_{(i,j)\in\mathcal{G}} x_{ij} = A, \tag{1a}$$

$$\sum_{(i,j)\in\mathcal{G}} y_{ij} = E, \tag{1b}$$

$$x_{ij} + y_{ij} \leq 1, \quad (i, j) \in \mathcal{G}. \tag{1c}$$

C. Shape Constraints

Economic viability aside, any practically deployable land-use plan must occupy *compact, hole-free, convex* regions. This section gives fully self-contained, rigorous constraints that enforce those three geometric properties on the discrete grid $\mathcal{G} = \{1, \dots, n_1\} \times \{1, \dots, n_2\}$. All constraints are stated for the agricultural indicator variables $\{x_{ij}\}$; an identical copy holds for the energy variables $\{y_{ij}\}$.

1) Discrete Euclidean Convexity: A continuous set is convex when it contains the entire segment joining any two of its points. On the integer grid we adopt the standard *lattice-segment* notion.

[Discrete convex set] A subset $\mathcal{A} \subseteq \mathcal{G}$ is *discretely convex* if for every pair of lattice points $p = (i, j)$ and $q = (i', j')$ in $\mathcal{A}$,

$$r \in \mathcal{G},\ r = \lfloor (1 - \lambda)p + \lambda q \rfloor \text{ for some } \lambda \in [0, 1] \implies r \in \mathcal{A}.$$

Equivalently (Hajnal's theorem), $\mathcal{A}$ is a lattice subset of the intersection of finitely many half-planes.

a) Half-plane encoding.: Let $\mathcal{H}$ be the finite family of all half-planes whose boundary passes through at least two distinct grid points. For $H \in \mathcal{H}$ write $\mathrm{in}_H(i,j) = 1$ if $(i,j) \in H$ and 0 otherwise. A lattice subset $\mathcal{A}$ is convex iff there exists a sub-family of half-planes $\{H_\ell\}_{\ell=1}^{L} \subseteq \mathcal{H}$ such that

$$(i,j) \in \mathcal{A} \iff (i,j) \in H_\ell \quad \forall \ell.$$

Introduce binary activation variables $z_\ell \in \{0,1\}$ for the half-planes and enforce (for every cell (i,j))

$$x_{ij} \le z_\ell + \big(1 - \mathrm{in}_{H_\ell}(i,j)\big), \quad \forall \ell. \tag{2}$$

Constraint (2) guarantees that if a cell is selected ($x_{ij} = 1$) then it satisfies all active ($z_\ell = 1$) half-planes, hence the selected set is convex. Finally, convexity requires every active half-plane to cut out at least one lattice point:

$$\sum_{(i,j)} x_{ij}\, \mathrm{in}_{H_\ell}(i,j) \;\ge\; z_\ell, \quad \forall \ell. \tag{3}$$

The family $\mathcal{H}$ has polynomial cardinality $\mathcal{O}(N^2)$; constraints (2)–(3) are therefore finite and linear.

Although large, the half-plane formulation is *exact*: any violation of convexity activates a separating half-plane that breaks either (2) or (3). Cutting-plane implementations add half-planes lazily, keeping the working model compact in practice.

2) Hole-Freeness (Simple Connectivity): Let $G = (\mathcal{G}, \mathcal{E})$ be the 4-neighbourhood grid graph.

[Hole-free set] A subset $\mathcal{A} \subseteq \mathcal{G}$ is *hole-free* if the complement $\mathcal{G} \setminus \mathcal{A}$ is connected in G.

Hole-freeness can be enforced by a single *max-flow* feasibility system of size $\mathcal{O}(N)$, originally due to Kolmogorov and Zabih [8]. We recall the constraints succinctly.

a) Flow variables.: Assign a unit source to every boundary cell with $x_{ij} = 0$ and a unit sink to every interior cell with $x_{ij} = 0$. Binary edge flows $f_{uv} \in \{0,1\}$ obey

$$0 \le f_{uv} \le 1, \qquad uv \in \mathcal{E}, \tag{4}$$

$$\sum_{v:(u,v)\in\mathcal{E}} f_{uv} \;-\; \sum_{v:(v,u)\in\mathcal{E}} f_{vu} = b_u - h_u, \qquad u \in \mathcal{G}, \tag{5}$$

where $b_u \in \{-1, 0, 1\}$ is the prescribed supply/demand and $h_u \in \{0,1\}$ is a binary slack that equals 1 iff node u lies in an uncovered hole. Penalising $\sum_u h_u$ in the Hamiltonian drives every feasible optimum towards $h_u = 0$ for all u, thereby eliminating holes.

Summary. Constraints (2)–(3) ensure that every chosen region is discretely convex, while (4)–(5) (with hole penalties) guarantee simple connectivity. Together they yield land-use patches that are *convex, compact, and free of interior voids*, satisfying the operational requirements for large-scale agricultural and energy installations.

D. Utility Maximisation

For each cell $(i,j) \in \mathcal{G}$ we define a *local utility* that reflects how well its heat-map score matches the land use assigned to it:

$$u_{ij}(x_{ij}, y_{ij}) \;=\; (1 - H_{ij})\, x_{ij} + \; H_{ij}\, y_{ij}, \qquad (i,j) \in \mathcal{G}.$$

A cell that is cool ($H_{ij} \approx 0$) contributes most when dedicated to agriculture ($x_{ij} = 1$), whereas a hot cell ($H_{ij} \approx 1$) yields maximal gain when assigned to energy production ($y_{ij} = 1$).

Collecting all decision variables in $x = \big(x_{ij}\big)_{(i,j)\in\mathcal{G}}$, $y = \big(y_{ij}\big)_{(i,j)\in\mathcal{G}}$, our goal is to solve the binary programme

$$\max_{x,y\in\{0,1\}^{\mathcal{G}}} \sum_{(i,j)\in\mathcal{G}} u_{ij}(x_{ij}, y_{ij}) \quad \text{subject to} \quad \begin{cases} (1) \text{ (quotas \& exclusivity)}, \\ \text{Discrete convexity constraints (2)–(3)}, \\ \text{Hole-freeness constraints (4)–(5)}. \end{cases} \tag{6}$$

Even when the energy quota is set to zero ($E = 0$) and the shape constraints are dropped, (6) reduces to selecting A out of N unit-weight items so as to maximise $\sum_{(i,j)}(1 - H_{ij})\, x_{ij}$, which is the SUBSET-SUM/KNAPSACK problem with unit weights—known to be NP-hard. Hence the full problem (6), augmented with convexity and hole-freeness, remains NP-hard; one cannot in general expect polynomial-time exact algorithms unless P = NP.

E. Quadratic HUBO Encoding

We cast optimisation problem (6) into a *quadratic higher-order unconstrained binary optimisation* (HUBO) instance, so that any global minimiser of the Hamiltonian coincides with an optimal land-use assignment.

1) Penalty Variables:

a) (i) Discrete–convexity penalties.: Recall the finite family of half-planes $\mathcal{H} = \{H_\ell\}_{\ell=1}^{L}$ introduced in §IV-C. For each H_ℓ we add

- an *activation binary* $z_\ell \in \{0, 1\}$ indicating that the half-plane is enforced;
- a slack variable $s_{ij\ell} \in \{0, 1\}$ for every cell $(i, j) \in \mathcal{G}$, capturing a possible violation of H_ℓ at that cell.

b) (ii) Hole-freeness penalties.: As in §IV-C, let

- $h_{ij} \in \{0, 1\}$, marking whether (i, j) lies in a residual interior hole;
- $f_{uv} \in \{0, 1\}$, the unit-capacity flow on each edge $uv \in \mathcal{E}$ of the 4-neighbourhood graph.

2) Hamiltonian: Choose constants $\lambda_1, \dots, \lambda_7 > 0$ strictly larger than $\max_{(i,j)} u_{ij}(1,0)$ (the peak gain of a single cell). Define the quadratic Hamiltonian

$$\begin{aligned}
\mathcal{H}(x,y,z,s,h,f) = &- \sum_{(i,j)\in\mathcal{G}} u_{ij}(x_{ij}, y_{ij}) && \text{(utility)}\\
&+ \lambda_1\Big(A - \sum_{(i,j)} x_{ij}\Big)^2 + \lambda_2\Big(E - \sum_{(i,j)} y_{ij}\Big)^2 + \lambda_3 \sum_{(i,j)} x_{ij} y_{ij} && \text{(quotas \& exclusivity)}\\
&+ \lambda_4 \sum_{\ell=1}^{L} \sum_{(i,j)\in\mathcal{G}} \big(x_{ij} - z_\ell - (1 - \mathrm{in}_{H_\ell}(i,j)) - s_{ij\ell}\big)^2 && \text{(half-plane adherence)}\\
&+ \lambda_5 \sum_{\ell=1}^{L} \Big(z_\ell - \sum_{(i,j)\in\mathcal{G}} x_{ij}\,\mathrm{in}_{H_\ell}(i,j)\Big)^2 && \text{(non-empty active half-planes)}\\
&+ \lambda_6\,\mathrm{FlowLP}(x,h,f) + \lambda_7 \sum_{(i,j)\in\mathcal{G}} h_{ij}. && \text{(hole elimination)}
\end{aligned}$$

Every term in (hole elimination) is quadratic: each square expands into constants, linear, and bilinear products of binary variables, never introducing degree > 2 monomials.

3) Exactness Guarantee: Let the penalty multipliers satisfy $\lambda_1, \dots, \lambda_7 > \max_{(i,j)} u_{ij}(1,0)$. Then every global minimiser of $\mathcal{H}$ is an optimal solution of problem (6), and vice versa.

Feasibility. Any violation of a hard constraint from (6) (quotas, exclusivity, discrete convexity, hole-freeness) activates at least one penalty term in rows (2)–(5) or (6)–(7) of (hole elimination), incurring cost $\geq \lambda_1$, strictly larger than the maximal change in utility that can be gained by flipping a single variable. Hence no infeasible assignment minimises $\mathcal{H}$.

Optimality on the feasible set. For a feasible assignment every penalty vanishes, and $\mathcal{H}$ equals $-\sum u_{ij}$. Therefore minimising $\mathcal{H}$ over the feasible set is equivalent to maximising the utility in (6). Combining feasibility and optimality yields the claimed one-to-one correspondence.

Hamiltonian (hole elimination) is a genuine *quadratic HUBO*. Two classes of solvers are thus directly applicable:

1) **Quantum annealers** (e.g. D-Wave, Rigetti) after standard minor-embedding of the quadratic graph.
2) **Ising-style classical optimisers.** In particular we deploy the *Iskay* library by KIPU QUANTUM, a GPU-accelerated implementation of the parallel tempering with isoenergetic cluster moves (PT+ICM) meta-heuristic. Empirically, Iskay reaches ground-state energies on QUBO sizes up to a few hundred thousand variables in minutes, outperforming current publicly available quantum annealers by 1–2 orders of magnitude in wall-time while avoiding embedding overheads. The present formulation enlarges the variable set only polynomially in N, fitting comfortably within Iskay's memory footprint (16–32 GB GPUs).

Because Iskay runs on commodity GPU clusters, it offers a more resource-efficient path to high-quality solutions than near-term quantum hardware, yet remains algorithmically faithful to the Ising paradigm—making it straightforward to switch to quantum back-ends once hardware matures.

REFERENCES

[1] B. Stray, X. Bosch-Lluis, R. Thompson, C. Okino, N. Yu, N. Lay, B. Muirhead, J. Hyon, H. Leopardi, P. Brereton, A. Mylapore, B. Loomis, S. Luthcke, P. Ghuman, S. Bettadpur, M. D. Lachmann, T. Stolz, C. Kuehl, D. Weise, H. Ahlers, C. Schubert, A. Bawamia, and S.-w. Chiow, "Quantum gravity gradiometry for future mass change science," *EPJ Quantum Technology*, vol. 12, no. 1, p. 35, 2025.

[2] D. Maheshwari, D. Sierra-Sosa, and B. Garcia-Zapirain, "Variational quantum classifier for binary classification: Real vs synthetic dataset," *IEEE Access*, vol. 10, pp. 3705–3715, 2022.

[3] M. Norimoto, R. Mori, and N. Ishikawa, "Quantum algorithm for higher-order unconstrained binary optimization and mimo maximum likelihood detection," *arXiv preprint arXiv:2205.15478*, 2022, accepted for publication in IEEE Transactions on Communications.

[4] Food and Agriculture Organization of the United Nations, "Guidelines on sustainable crop production in arid and semi-arid zones," Rome, 2022, accessed 27 Apr 2025. [Online]. Available: https://www.fao.org/3/i2216e/i2216e.pdf

[5] G. Kucsko, P. C. Maurer, and N. Y. Y. et al., "Nanometre-scale thermometry in a living cell," *Nature*, vol. 500, pp. 54–58, 2013.

[6] B. Stray, A. Lamb, A. Kaushik, J. Vovrosh, A. Rodgers, J. Winch, F. Hayati, D. Boddice, A. Stabrawa, A. Niggebaum, M. Langlois, Y.-H. Lien, S. Lellouch, S. Roshanmanesh, K. Ridley, G. de Villiers, G. Brown, T. Cross, G. Tuckwell, A. Faramarzi, N. Metje, K. Bongs, and M. Holynski, "Quantum sensing for gravity cartography," *Nature*, vol. 602, no. 7898, pp. 590–594, 2022.

[7] P. Rebentrost, M. Mohseni, and S. Lloyd, "Quantum support vector machine for big data classification," *Phys. Rev. Lett.*, vol. 113, p. 130503, Sep 2014. [Online]. Available: https://link.aps.org/doi/10.1103/PhysRevLett.113.130503

[8] V. Kolmogorov and R. Zabih, "What energy functions can be minimized via graph cuts?" *IEEE Transactions on Pattern Analysis and Machine Intelligence*, vol. 26, no. 2, pp. 147–159, 2004.